Title
Target-wide Induction and Synapse Type-Specific Robustness of Presynaptic Homeostasis

Journal
Current Biology, 29(22)

ISSN
0960-9822

Authors
Genç, Özgür
Davis, Graeme W

Publication Date
2019-11-01

DOI
10.1016/j.cub.2019.09.036

Peer reviewed

Published in final edited form as:

Curr Biol. 2019 November 18; 29(22): 3863–3873.e2. doi:10.1016/j.cub.2019.09.036.

Target-Wide Induction and Synapse Type-Specific Robustness of Presynaptic Homeostasis

Özgür Genç[1], **Graeme W. Davis**[1,2]

[1]Department of Biochemistry and Biophysics, Kavli Institute for Fundamental Neuroscience, University of California, San Francisco, San Francisco, CA 94158

Summary

Presynaptic homeostatic plasticity (PHP) is an evolutionarily conserved form of adaptive neuromodulation, observed at both central and peripheral synapses. We make several fundamental advances, interrogating the synapse-specificity of presynaptic homeostatic plasticity. We define how PHP remains robust to acute versus long-term neurotransmitter receptor perturbation. We describe a general property of PHP, which includes global induction and synapse-specific expression mechanisms. Finally, we detail a novel synapse-specific expression mechanism for PHP that enables the conversion from short to long-term PHP expression. If our data can be extended to other systems, including the mammalian central nervous system, it suggests that PHP can be broadly induced and expressed to sustain the function of complex neural circuitry.

eTOC:

Genc and Davis interrogate the synapse specificity of presynaptic homeostasis, demonstrating that all synapses at which postsynaptic neurotransmitter receptors are perturbed express PHP, thereby supporting a global induction mechanism. However, different synapse types contacting a single target can differentially express homeostatic plasticity.

Keywords

motoneuron subtypes; MN-1b; MN-1s; phasic and tonic transmission; presynaptic homeostatic plasticity; synaptic transmission; calcium channels; active zone organization

*Correspondence: Graeme.davis@ucsf.edu.

[2]Lead contact

Author contributions

Ö.G., project design, data collection, data analysis, interpretation, co-writing and editing the manuscript; G.W.D., project design, data interpretation, writing the manuscript.

Declaration of Interests

The authors declare no competing interests.

Introduction

Presynaptic homeostatic plasticity (PHP) is evolutionarily conserved from insects to rodents and human [1]. PHP is expressed at the glutamatergic synapses of the *Drosophila* neuromuscular junction (NMJ) following the perturbation of post-synaptic glutamate receptors (GluR), and is similarly expressed at the cholinergic NMJ of rodents and humans [2,3]. PHP is not restricted to peripheral neuromuscular synapses. PHP also can be induced by prolonged activity blockade in primary neuronal cell culture [4,5]. In every instance, PHP is expressed as an increase in presynaptic neurotransmitter release due to an increase in presynaptic calcium influx and a parallel expansion of the readily-releasable pool of synaptic vesicles [1,6].

A major outstanding question concerns whether the mechanisms of PHP are synapse-specific. Nearly twenty years ago, it was demonstrated that PHP can be expressed in a target specific manner at the terminals of a single neuron [7]. This basic discovery was recently revisited and confirmed with an independent, target-specific manipulation [8]. These data do not, however, speak to the specificity of PHP among synapses that contact a single target cell. The importance of this issue can be best appreciated by considering the complex innervation of individual central neurons. A hippocampal neuron can receive thousands of presynaptic inputs [9]. If the target neuron is perturbed, it remains unknown whether every presynaptic input contacting that target cell is induced to express PHP. Indeed, it is unclear whether every synapse is capable of expressing PHP. Answering this question is essential for understanding whether PHP universally stabilizes synaptic transmission following a postsynaptic perturbation, or whether PHP might alter the differential flow of information through neural circuitry by stabilizing specific subsets of synapses.

The *Drosophila* NMJ is a model system where the specificity of PHP induction and expression can be directly addressed. Nearly every muscle in larval peripheral nervous system is innervated by two motoneurons, one referred to as *tonic* and the other *phasic* based on different, characteristic initial release probabilities [10]. There have been recent attempts to explore the synapse-specific expression of PHP at tonic versus phasic terminals on single muscle targets in *Drosophila* [11-14]. Synapse-specific changes in protein abundance, associated with the expression of PHP have been documented, but it remains uncertain whether these alterations are causal for the expression of PHP [11-13]. A separate study used optical quantal analysis, employing a postsynaptically expressed, genetically encoded calcium indicator (GCaMP) to assess the synapse-specificity of PHP. This study concluded that PHP is expressed exclusively at tonic nerve terminals, even though postsynaptic glutamate receptors are disrupted at all nerve terminals (phasic and tonic) contacting a single target [14]. If this model is correct, then the homeostatic increase in release at tonic terminals must be very large, completely offsetting a perturbation that affects both the phasic and tonic terminals. Furthermore, phasic and tonic terminals have different release properties, expressing different short-term dynamics of release during repetitive stimulation. It is well-established that PHP is achieved without altering the short-term dynamics of presynaptic release, when phasic and tonic synapses are stimulated simultaneously [15-17]. This observation implies that PHP is expressed equivalently at phasic and tonic terminal. By contrast, if PHP is expressed exclusively by tonic terminals, then the induction of PHP

should cause tonic synapses to dominate neurotransmission and release dynamics should shift to reflect a larger role of the tonic synapse, something that is not observed [15-17]. These questions prompted us to revisit the topic of synapse-specificity.

We employ new methods to study synapse-specific homeostatic plasticity, combining optical stimulation of single nerve terminals with electrophysiological quantification of synaptic transmission. We demonstrate that PHP is universally induced at all synapses contacting a single muscle target, inclusive of both phasic and tonic nerve terminals, contrasting with previously published data [14]. However, we do uncover evidence that the expression of PHP can differ at phasic and tonic nerve depending upon the concentration of external calcium and the acute versus long-term mechanisms of PHP induction. The differential expression of PHP, dependent upon specific recording conditions, can fully account for prior claims of synapse-specific PHP. Based on our findings, we propose a new model to account for the global expression of PHP at different synapse types, and the transition from acute to chronic expression of PHP.

Results

Optogenetic dissection of synaptic inputs at *Drosophila* neuromuscular junction

Two types of motoneurons, MN-1b and MN-1s form synapses at *Drosophila* larval muscles. These inputs have been previously mapped by dye-filling individual motoneurons in the ventral nerve chord and tracing their axons and terminals to specific muscle targets [10,18]. More recently, analysis of individual motoneurons has been enabled by the identification of highly specific GAL4 drivers [19].

We took advantage of previously characterized GAL4 drivers [19-21] and optogenetic reagents [22,23] to functionally isolate two glutamatergic neurons, MN-1b and MN-1s, that innervate muscles 6 and 7 in the larval periphery. We verified the specificity of each GAL4 line by expressing *UAS-CD8-GFP*, revealing MN-1b and MN-1s specific labeling at muscles 6 and 7 (Figure 1A). Next, we drove the expression of channelrhodopsin (*UAS-ChR2*^{T159C}) using the MN-1s or MN-1b specific drivers (Figure 1B). Following a brief wide-field illumination pulse (470nm, 3ms), we record robust excitatory postsynaptic potentials (EPSPs) (Figure 1C-D, shown for MN-1b input) which were completely blocked by the application of the sodium channel blocker, tetrodotoxin (TTX) (Figure 1D, right). We also measured the light intensity threshold that is necessary to evoke EPSPs and demonstrate that EPSPs are recruited in an all-or-none fashion, consistent with optical triggering of a presynaptic action potential (Figure 1E, shown for MN-1b input, EPSCs at 3 mM Ca^{2+}). We further tested ChR2-mediated activation of synaptic inputs using the ultrasensitive variant of channelrhodopsin, ReachR, which allowed us to perform 2-photon laser spiral scanning at the single bouton level. Bouton-level illumination of the synapse also provided a robust EPSPs recorded in muscle 6 (Figures 1F-H). Spiral scan illumination-induced responses were also blocked by the application of TTX (Figures 1G). Overall, this data verifies that excitation of the NMJ by ChR2 is able to generate action potential induced neurotransmitter release.

Next, we quantified the magnitude of EPSPs and EPSCs induced by selective, optogenetic stimulation of each motoneuron contacting muscle 6. Stimulation of MN-1s evoked EPSPs that were 50% larger than those evoked following stimulation of MN-1b, recorded in muscle 6 at 0.5 mM extracellular calcium concentration (Figure 1I-K, 25.7± 2.2 mV for 1s; 15.6±1.3 mV for MN-1b, $p<0.01$). This result confirms previous findings that MN-1b synapses have smaller synaptic output compared to MN-1s synapses [24-26]. To obtain the full-extent of the neurotransmitter release at each synapse, we switched to two-electrode voltage-clamp and recorded excitatory post-synaptic currents (EPSC) at an elevated extracellular calcium concentration (3.0 mM). Before quantifying EPSCs, we ensured that electrically-induced EPSCs and ChR2-induced EPSCs share similar kinetic properties. To do so, we used electrical stimulation and set the electrical intensity threshold to isolate MN-1b fibers [26]. Then, we evoked EPSCs by light-illumination of *UAS-ChR2*^{T159C} expressed in MN-1b (Figure S1A). EPSC kinetics are identical comparing electrical and optical stimulation (Figure S1B).

Next, we quantified light-evoked responses, comparing MN-1s and MN-1b synapses at elevated extracellular calcium concentrations, ranging from 0.5 to 3.0 mM. EPSCs initiated by stimulating either synaptic input were similar, (Figure 1L-N, 165.1± 8.5 nA for 1s; 165.4±11.8 mV for 1b, $p>0.5$) when recordings were made at muscle 6. Then, we repeated the experiment at the synapses contacting a different muscle (muscle 1, M1) (Figure S2A). A different MN-1b driver was used that is exclusively expressed in the MN-1b neuron contacting muscle 1 (MN-1b, 40701 [19]). At low extracellular calcium concentration (0.5mM), we also observed that MN-1b mediated EPSPs were smaller compared to MN-1s EPSPs (Figures S2B-D, 9.3± 1.1 mV for MN-1s; 5.8±0.7 mV for MN-1b $p<0.05$). Whereas, when we elevated the extracellular calcium to 3.0 mM, MN-1b inputs were stronger, almost two-fold larger compared to MN-1s inputs (Figures S2E-G, 46.3± 1.5 nA for MN-1s; 88.7± 5.1 nA for MN-1b $p<0.0001$). This suggests that calcium sensitivity of release is smaller at MN-1b tonic synapses, whereas increasing extracellular calcium can elevate the release rate of MN-1b synapses equal to or greater than the levels of MN-1s phasic synapses. Having defined the release properties of MN-1b and MN-1s synapses using optogenetic stimulation, we moved to address the synapse specificity of presynaptic homeostatic plasticity.

MN-1b and MN-1s both participate in acute induction and expression of homeostatic plasticity

Presynaptic homeostatic plasticity can be rapidly induced by application of sub-blocking concentrations of the glutamate receptor antagonist philanthotoxin (PhTx) [27]. PhTx binds to glutamate receptors and causes a reduction in ionic conductance which leads to a decrease in average miniature excitatory postsynaptic potential (mEPSP) amplitude (Figure 2A). In this protocol, a 10-minute incubation of *Drosophila* third instar larvae with PhTx is sufficient to induce and express presynaptic homeostatic plasticity via an increase in presynaptic neurotransmitter release [15,27-29].

First, we tested the contribution of MN-1s and MN-1b synapses during the acute induction and expression of homeostatic plasticity at the NMJ. Following application of PhTx, MN-1s neurons showed a robust, homeostatic increase in quantal content (Figure 2A-B, 175% of

baseline, $p<0.001$) at 0.5 mM extracellular calcium. When quantal content is plotted against mEPSP amplitudes (+/− PhTx) for each recording, a clear negative correlation is observed (Figure 2C, $R^2=0.63$) demonstrating robust expression of PHP at the MN-1s synapse (see [17,27]). By comparison, the expression of PHP at the MN-1b synapse was less robust, being more variable and smaller in average magnitude (Figure 2D). On average, mEPSPs are significantly decreased and there is a statistically significant, homeostatic increase in quantal content (Figure 2E; 145% of baseline, $p<0.01$). However, when quantal content is plotted against mEPSP amplitude, although there is a negative correlation, the correlation is substantially weaker than that observed for the MN-1s synapse (Figure 2F, $R^2=0.23$).

Next, we switched to two-electrode voltage clamp and raised the extracellular calcium concentration to 3.0 mM, a concentration at which release probability has plateaued to a maximum [16]. In this condition, the MN-1b and MN-1s synapses showed equivalent, highly robust PHP (Figure 2G-H and 2J-K; MN-1s, 175% homeostatic increase; MN-1b, 178% homeostatic increase; $p<0.01$ for each comparison to baseline in the absence of PhTx). The robustness of PHP is also verified when quantal content is plotted against mEPSP amplitudes (Figures 2I and 2L; $R^2=0.71$ for MN-1s, $R^2=0.55$ for MN-1b). Again, the MN-1s correlation is stronger than that observed for MN-1b, but the MN-1b at 3.0 mM [Ca^{2+}] reveals a stronger correlation than that observed at low extracellular calcium. Finally, we repeated the same set of experiments using another MN-1s specific GAL4 driver, *MN-1s^{ShakB}-GAL4* [21]. Expression of *UAS-ChR2^{T159C}* by *ShakB-GAL4* gave similar EPSP and EPSC amplitudes compared to the MN-1s^{49722} driver (Figure S3), confirming that the GAL4 driver does not quantitatively affect our measurements. In addition, when we tested PhTx-induced homeostasis, the magnitude of potentiation was also similar both at low and high extracellular calcium concentrations (Figures S3B and E) as compared to MN-1s^{49227}.

Two additional controls were performed. First, we controlled for synapse specific effects of PhTx application (Figure S4). To do so, we selectively stimulated either MN-1b or MN-1s prior to and following the application of PhTx. We assessed EPSP amplitudes 30s following PhTx application, a time point prior to the induction of PHP. This allowed us to determine the magnitude of the PhTx-dependent perturbation selectively at MN-1b and MN-1s terminals. We demonstrate that both terminals show a strong PhTx-dependent reduction in EPSP amplitude (54% reduction at MN-1b and 42% reduction at MN-1s). Thus, each synapse is similarly perturbed by PhTx application, with a slight bias toward MN-1b consistent with prior evidence that GluRIIA immunostaining is enriched at MN-1b terminals [30]. Second, we repeated experiments in 1.8mM external calcium, likely reflecting physiological calcium. Again, PHP is robustly induced at both MN-1b and MN-1s (Figure S5).

Taken together, these data demonstrate that MN-1b and MN-1s both participate in presynaptic homeostatic plasticity following a global impairment of postsynaptic glutamate receptors. We conclude that PHP is globally induced and expressed by MN-1b and MN-1s. We further propose that smaller release probability inherent to the MN-1b synapse renders the expression of PHP less robust when recordings are made at low extracellular calcium concentrations. Thus, the expression of PHP can be synapse-specific and condition specific,

an effect that correlates with basal presynaptic release probability, but which may reflect more specific differences in the molecular composition or architecture of presynaptic release sites.

MN-1b and MN-1s both participate in chronic expression of homeostatic plasticity

While an acute block of receptors leads to an expression of homeostasis on time scales of ~10 minutes, genetic deletion of the GluRIIA subunit of glutamate receptors causes a sustained reduction in quantal amplitudes throughout the life of a larvae [31], which is interpreted to reflect the long-term, chronic expression of PHP. The long-term expression of PHP is believed to require transcription and translation, as it is selectively affected by mutations in the transcription factors *gooseberry (Pax6* ortholog) and *Relish* (Rel-domain transcription factor) [32,33]. Furthermore, presynaptic ENaC channel subunits, which are necessary for the long-term expression of PHP, show increased transcript and protein level in the *GluRIIA* mutant background [34]. However, it remains unknown whether new transcription and translation simply consolidate the expression of PHP, or whether the long-term expression of PHP involves a new mechanism of expression.

Initial experiments revealed a significant surprise. At low extracellular calcium levels (0.5 mM), we found that PHP is completely absent at MN-1s synapses (Figure 3A-B, 101% baseline, $p>0.1$, Figure 3C, $R^2=0.0002$) whereas presynaptic homeostasis is expressed at MN-1b synapses. The mEPSP and quantal content has a correlation similar to that observed during the PhTx-dependent rapid induction of PHP at the MN-1b synapse (Figure 3D-E, 173% baseline, $p<0.001$, Figure 3F, $R^2=0.27$). Thus, the participation of the MN-1s synapse during PHP changes dramatically when we compare the rapid induction of PHP (Figure 2) and the long-term expression of PHP (Figure 3). Note that the *GluRIIA* transcript is only expressed in muscle, and cannot account for the difference we observe [31]. Furthermore, it should be noted that the GluRIIA protein is expressed at both the MN-1s and MN-1b nerve terminals. It appears that the expression of PHP remains synapse-specific at low extracellular calcium, but it completely switches, relying on MN-1s following PhTx and relying on MN-1b in the *GluRIIA* mutant background.

Next, we elevated extracellular calcium to 3.0 mM and, again, tested for the expression of PHP. At elevated extracellular calcium, the MN-1s synapse fully expressed PHP (Figure 3G-H, 213% baseline, $p<0.001$, Figure 3I, $R^2=0.69$). The MN-1b synapse also demonstrated robust expression of PHP (Figure 3J-K, 188% baseline, $p<0.001$, Figure 3L, $R^2=0.66$). The magnitude and robustness of PHP were similar at the MN-1b and MN-1s synapses. This result demonstrates that PHP is uniformly induced at the MN-1b and MN-1s synapses, consistent with GluRIIA being present at both synapses in the wild type animal and, by extension, both synapses being perturbed in the *GluRIIA* mutant. However, the failure to induce PHP at the MN-1s synapse cannot be accounted for by a lower initial release probability at baseline, as proposed for the failure of MN-1b synapses to fully express PHP following PhTx. Clearly, there are synapse-specific differences in the expression of PHP. These synapse-specific expression mechanisms differ depending upon how PHP is induced, acute versus chronic, and cannot be easily explained by differential initial release

probabilities. Therefore, we characterized the differences in presynaptic release that might correlate with synapse-specific expression of PHP.

EGTA-sensitive calcium domains contribute expression of PHP in *GluRIIA* mutants

First, we repeated the experiments in *GluRIIA* mutants, by electrical stimulation of both MN-1s and MN-1b, and tested whether PHP becomes more robust with increasing extracellular calcium concentration. We electrically stimulated the nerve fiber with suprathreshold intensities to recruit both 1b and 1s inputs. At low extracellular calcium concentration (0.3 mM), we observed clear evidence of PHP (Figures 4A-B, 205% of baseline, $p<0.05$) and a strong negative correlation of mEPSP and quantal content, as expected (Figure 4C, $R^2=0.51$). When we elevated the extracellular calcium to 3.0 mM, PHP became more robust, with a larger magnitude (Figure 4D-E, 250% of baseline, $p<0.001$) and stronger negative correlation when plotting mEPSP versus quantal content (Figure 4F, $R^2=0.82$). Thus, in *GluRII* mutants, the robustness of PHP improved as a function of increased extracellular calcium, whether the experiment is performed by stimulating both neurons independently using ChR2, or stimulating both neurons simultaneously using electrical stimulation.

How is it possible that PHP becomes more robust upon increasing extracellular calcium concentration? One possibility is that vesicles become functionally more tightly coupled to presynaptic calcium channels as extracellular calcium concentrations rise. To test this hypothesis, we used a calcium chelator, EGTA-AM, which has slow calcium-binding kinetics [35] and prevents the recruitment of loosely-coupled vesicles for fusion [29,36]. We first tested whether the acute induction of PHP is sensitive to EGTA-AM. We found that MN-1b and MN-1s synapses, following the induction of PHP, showed no differential sensitivity to EGTA-AM treatment, quantified as no change in average EPSC amplitude (Figure 4G, I, 92% for 1s, $p>0.1$ 100% for 1b, $p>0.1$). Next, we tested the EGTA-AM sensitivity of synapses in *GluRIIA* mutants. Contrary to acute inhibition with PhTx, *GluRIIA* mutants, both the MN-1s and MN-1b synapses, were sensitive to EGTA-AM (Figure 4G-I, 72% for 1s, $p<0.01$, 69% for 1b, $p<0.01$). We verified this phenomenon by recruiting both inputs with electrical stimulation. We also saw a significant drop in EPSC amplitudes when preincubated with EGTA-AM ($p<0.001$, Figure 5A). Increased sensitivity to EGTA-AM suggests that there is a significant portion of synaptic vesicles located at a distance from presynaptic calcium channels in *GluRIIA* mutants. Chelating calcium prevents these distant vesicles from fusing, which in turn, suppresses EPSC amplitudes evoked with a single action potential. It appears that there has been a re-organization of the presynaptic release site during the long-term expression of PHP, and this re-organization occurs at both MN-1s and MN-1b.

It was previously demonstrated that glutamate receptor perturbation induces recruitment of PPK channels, which subsequently leads to increases in calcium influx at the presynaptic terminal [28]. Therefore, we also tested whether EGTA-AM-sensitive calcium domains in *GluRIIA* mutants are sensitive to PPK activity. When we applied a PPK channel inhibitor (benzamil, 50 μM) to larvae previously incubated with EGTA-AM, we saw a decrease in EPSC amplitudes that was slightly larger than those treated with EGTA alone (34% vs 22%,

p<0.01, Figure 5A-B). We also tested benzamil alone on *GluRIIA* mutants, and we saw a similar drop in EPSC amplitudes as compared to benzamil plus EGTA-AM (32% vs 34%, p>0.1, Figure 5A-B). Since the action of benzamil is not additive with EGTA-AM, it suggests that the two treatments converge on the same process, the homeostatic increase in vesicle fusion. The insertion of presynaptic ENaC channels drives increased presynaptic calcium influx per action potential as shown previously [15,28,37]. This occurs during both the rapid induction and sustained expression of PHP. Thus, we have identified calcium-dependent, perturbation specific expression of PHP, effects that are summarized in Figure 5C-D. We propose that, in *GluRIIA* mutants, the presynaptic release sites are modified such that neurotransmitter release and PHP become EGTA-AM sensitive. This may reflect a re-organization of the presynaptic active zone, creating over-lapping calcium domains and enhanced vesicle release (Figure 5D). Accordingly, the failure of PHP at MN-1s synapses in the *GluRIIA* mutant might reflect the different organization of active zones at a phasic synapse, such that over-lapping calcium domains cannot occur at low extracellular calcium, and PHP expression selectively fails at this synapse in the *GluRIIA* mutant.

Discussion

We have taken advantage of cell-type specific GAL4 drivers to achieve selective, optogenetic stimulation of single motoneuron inputs to a single muscle fiber. This has enabled us to explore the synapse-specificity of presynaptic homeostatic plasticity. We demonstrate that the global disruption of postsynaptic glutamate receptors, either pharmacologically or genetically, induces robust presynaptic homeostatic plasticity at both tonic and phasic presynaptic terminals contacting a single muscle target. The fact that both phasic and tonic synapses participate in presynaptic homeostasis is consistent with previously published work demonstrating that the expression of PHP does not alter the short-term dynamics of presynaptic release when both the phasic and tonic synapses are stimulated simultaneously [15,17].

We also demonstrate that PHP is differentially expressed at phasic and tonic synapses when external calcium concentration is decreased. Remarkably, however, the synapse-specific effects of reducing external calcium depend upon how PHP is initiated. Acute induction of PHP is robustly expressed by the phasic, but not as robustly at tonic synapses. However, the situation completely reverses during chronic induction of PHP, where PHP is robustly expressed by the tonic, not phasic synapses (see summary in Figure 5C). These data highlight a novel, fundamental difference in the mechanisms responsible for the rapid versus prolonged expression PHP.

It was previously argued that PHP is synapse-specific, being expressed exclusively by the tonic nerve terminal [14]. These prior experiments included an optical quantal analysis of synaptic transmission in the *GluRIIA* mutant. Here, we confirm that PHP is expressed solely by the tonic synapse under conditions of diminished release, the *GluRIIA* mutant background and low external calcium (conditions that reflect those pursued in the prior optogenetic study which utilized high concentrations of external magnesium, presumably done to stabilize the optical recording conditions [14]). However, by exploring multiple methods of PHP induction at multiple external calcium concentrations, we clearly

demonstrate that PHP is globally induced and expressed, with differences in PHP expression emerging only when external calcium is diminished, and dependent upon how PHP is induced, acutely versus chronically.

Synapse-specific expression: release probability and access to weakly coupled vesicles

The current understanding of PHP expression is based primarily on the genetic deletion of key molecular components of the presynaptic homeostatic machinery, discovered in forward genetic screens. A presynaptic ENaC channel, composed of subunits transcribed by the *PPK11*, *PPK16* and *PPK1* genes, is necessary for both the rapid induction and sustained expression of PHP, driving increased calcium influx through the presynaptic CaV2.1 calcium channel [28]. ENaC channel function is required for both short and long-term PHP, and we now demonstrate that it functions at both phasic and tonic synapses. So, differential activity of the ENaC channel cannot account for synapse-specific PHP expression at low external calcium.

We propose that the differential expression of acute versus chronic PHP may relate to the EGTA sensitivity of presynaptic release. The chronic induction of PHP is differentially sensitive to EGTA, implying that the chronic expression of PHP includes a population of synaptic vesicles that are weakly coupled to presynaptic calcium channels. This finding could explain the differential synapse-specific expression of PHP at phasic and tonic synapses. During the acute induction of PHP, low-release probability tonic synapses release neurotransmitter less efficiently at low external calcium, and PHP expression is correspondingly impaired. During the chronic induction, we propose that there is a transformation of the release site, allowing the participation of weakly coupled vesicles in the release process. We hypothesize that the different anatomical geometry of release sites, comparing phasic and tonic synapses [26], causes PHP to selectively fail at phasic synapses. More specifically, phasic synapses may be organized in such a way that weakly coupled vesicles cannot be accessed when external calcium is diminished. Such an effect would only be observed following the chronic induction of PHP combined with diminished external calcium.

Implications for the homeostatic stabilization of neural function in complex circuitry

The trigger that initiates PHP, whether acute or chronic, is the loss or inhibition of postsynaptic neurotransmitter receptors, whether considering the glutamatergic *Drosophila* NMJ or the cholinergic mammalian NMJ. Based upon the data that we present here, it appears that any synapse at which postsynaptic receptors are perturbed will express PHP. However, it has yet to be determined whether selective disruption of glutamate receptors at one synapse on a given target will induce synapse-selective PHP. The tools to achieve this experiment in a clearly reproducible manner do not yet exist. If PHP is expressed at every synapse that becomes perturbed, then PHP should stabilize the flow of information through complex neural circuitry. The related question of synapse-specific induction will determine whether information transfer can be selectively sustained through the regulation of some, but not all, synapses on a given target. Finally, our data suggest that some synapses may be more or less efficient at expressing PHP, acutely and chronically. We note that the tonic synapse always expresses PHP in a more variable manner. There is a large range of synapse types

with different release probabilities throughout the complex neural circuitry in the mammalian CNS, suggesting that PHP could be more or less robustly expressed at different synapses. As such, we may expect that the global induction of PHP could differentially affect neural circuit function in previously unsuspected ways, a possibility that could be important for considering the action of chronically administered neural therapeutics or drugs of addiction.

STAR METHODS

LEAD CONTACT AND MATERIALS AVAILABILITY

Further information and requests for resources and reagents should be directed to and will be fulfilled by the Lead Contact, Graeme W. Davis (Graeme.davis@ucsf.edu). This study did not generate unique reagents.

EXPERIMENTAL MODEL AND SUBJECT DETAILS

Drosophila melanogaster fly stocks were raised in standard cornmeal media at 25°C. For optogenetic experiments, 1 mM all-trans-retinal (Sigma-Aldrich) was added to the media and flies kept in the dark. All experiments were performed with *Drosophila* third-instar larvae.

METHOD DETAILS

All flies are on the *w1118* genetic background. *dhb9-GAL4* line was a kind gift from Dr. James Skeath. *w; GMR94G06-Gal4*, *w; GMR27E09-Gal4*, *w; UAS-ChR2.T159C*, *w; UAS-ReaChR* were obtained from Bloomington Drosophila Stock Center. The $GluRIIA^{SP16}$ mutation [31], w; *UAS-mCD8:GFP* [38] and the *OK371-GAL4* [39] lines were previously published.

Optogenetic stimulation—For optogenetic stimulation of the motoneurons, an LED light source mounted on the epifluorescence light path of the microscope (Zeiss) and the blue light at 470 nm reflected directly onto the specimen through the 40X water immersion objective (Zeiss). LED is controlled by a T-Cube™ LED Driver, triggered by a TTL pulse delivered from Digidata 1440 D/A converter (Molecular Devices). Light intensity below the objective is measured by an optical power meter (Thorlabs). For the activation of ChR2, a power range between 5-20 mW/cm2 was used. For 2P-excitation of the ReachR, a Chameleon family 2p-laser (Coherent) tuned at 720 nm was used. 2p-laser was controlled by spiral scanning module of SlideBook 6 (Intelligent Imaging Inc.).

Electrophysiology—The *Drosophila* 3rd instar larvae were dissected in hemolymph-like-3 (HL3) saline solution. HL3 is composed of 70mM NaCl, 5mM KCl, 10mM $NaHCO_3$, 115mM sucrose, 4.2mM trehalose, 5mM HEPES; 10mM $MgCl_2$ and 0.5mM Ca (unless otherwise specified). Motoneuron fibers were cut from ventral nerve chord, and the fillet preparation was pinned to a Sylgard plate. Sharp electrode recordings were performed from abdominal muscle 6 (M6) and muscle 1 (M1). Data collected with a Multiclamp 900B amplifier and digitized with Digidata 1440, sampled with Clampex software. For the electrical stimulation of the afferent motoneurons, cut-end of the nerve fibers were sucked

by a glass pipette that was pulled and fire-polished with a final tip diameter <50 μm. To evoke an action potential at the motoneuron terminals, a minimal electrical stimulation was sent from a stimulus isolator (Isoflex) and stimulation intensity was raised 10-20% above the threshold to avoid action potential failures. Same logic was applied for optogenetic stimulation. For sharp electrode recordings, glass pipettes were pulled with a tip-resistance ranging between 8-25 MOhm, lower tip-resistance electrodes were used for current injection in voltage-clamp mode. Current-clamp mode was used to quantify resting-membrane potential (RMP), input-resistance (Rin), record EPSP and mEPSPs at 0.3-0.5 mM extracellular calcium concentration. Muscles with RMP below −60 mV or Rin below 4 MOhm were discarded, unless otherwise specified. Voltage-clamp recordings were done at 3.0 mM extracellular calcium with a muscle RMP clamped to −65 mV. Pharmacological reagents were applied according to previously described protocols. For acute induction and expression of PHP, Philanthotoxin (PhTx) was applied through a longitudinal cut across the abdomen and the larvae was incubated for 10 minutes. For EGTA-sensitivity experiments, larvae were incubated in a 25 μM EGTA, 0 mM calcium HL3 solution for 10 minutes then thoroughly washed with HL3. Benzamil (25-50 μM) and tetrodotoxin (1 μM) were directly applied to the recording chamber without any preincubation.

Immunohistochemistry of neuromuscular junction—Drosophila third-instar larvae were dissected in HL3 solution and fixed with Bouin's solution for 3-5 minutes. Fixed larvae were permeabilized with Triton-X and overnight incubated at 4 C with primary GFP antibody (1:500 concentration). Alexa-488 (1:500) and Cy3-HRP (1:100) conjugated secondary antibodies were used for 30-minute incubations at room temperature. Samples were mounted in Vectashield (Vector laboratories), imaged with an inverted microscope (Carl Zeiss, Axiovert 200), equipped with 100X objective (Carl Zeiss, Plan Apochromat, 1.4 NA) and a CCD camera (CoolSnap, Roper Scientific). Images were acquired via SlideBook 5 (Intelligent Imaging), subsequently deconvolved and projected with maximum intensity.

QUANTIFICATION AND STATISTICAL ANALYSIS

All data are presented as mean ± standard error of mean. To test the difference between two groups with the normal distribution, we used unpaired two-tailed Student's t-test. To compare groups, we used one-way ANOVA, followed by Dunnett's multiple comparisons. Statistical significance is denoted by asterisks, (n.s. >0.05, * $p \leq 0.05$, ** $p \leq 0.01$, *** $p \leq 0.001$, **** $p \leq 0.0001$). Pearson correlation coefficients were calculated following a linear-fit of the X-Y quantal size-quantal content data.

DATA AND CODE AVAILABILITY

This study did not generate any unique datasets or code.

Supplementary Material

Refer to Web version on PubMed Central for supplementary material.

Acknowledgements

Supported by NIH grant number R35NS097212 to G.W.D. We thank Rick Fetter for his comments on the manuscript.

References

1. Davis GW (2013). Homeostatic signaling and the stabilization of neural function. Neuron 80, 718–28. Available at: http://www.pubmedcentral.nih.gov/articlerender.fcgi?artid=3856728&tool=pmcentrez&rendertype=abstract [Accessed November 18, 2014]. [PubMed: 24183022]
2. Wang X, Pinter MJ, and Rich MM (2016). Reversible Recruitment of a Homeostatic Reserve Pool of Synaptic Vesicles Underlies Rapid Homeostatic Plasticity of Quantal Content. J. Neurosci 36, 828–36. Available at: http://www.ncbi.nlm.nih.gov/pubmed/26791213 [Accessed September 27, 2016]. [PubMed: 26791213]
3. Cull-Candy SG, Miledi R, Trautmann A, and Uchitel OD (1980). On the release of transmitter at normal, myasthenia gravis and myasthenic syndrome affected human end-plates. J. Physiol 299, 621–38. Available at: http://www.pubmedcentral.nih.gov/articlerender.fcgi?artid=1279245&tool=pmcentrez&rendertype=abstract [Accessed October 29, 2015]. [PubMed: 6103954]
4. Mitra A, Mitra SS, and Tsien RW (2012). Heterogeneous reallocation of presynaptic efficacy in recurrent excitatory circuits adapting to inactivity. Nat. Neurosci 15, 250–257. Available at: http://www.ncbi.nlm.nih.gov/pubmed/22179109 [Accessed June 28, 2019].
5. Jakawich SK, Nasser HB, Strong MJ, McCartney AJ, Perez AS, Rakesh N, Carruthers CJL, and Sutton MA (2010). Local Presynaptic Activity Gates Homeostatic Changes in Presynaptic Function Driven by Dendritic BDNF Synthesis. Neuron 68, 1143–1158. Available at: http://www.ncbi.nlm.nih.gov/pubmed/21172615 [Accessed January 31, 2017]. [PubMed: 21172615]
6. Davis GW, and Müller M (2014). Homeostatic Control of Presynaptic Neurotransmitter Release. Annu. Rev. Physiol Available at: http://www.annualreviews.org/doi/abs/10.1146/annurev-physiol-021014-071740 [Accessed January 20, 2015].
7. Davis GW, and Goodman CS (1998). Synapse-specific control of synaptic efficacy at the terminals of a single neuron. Nature 392, 82–86. Available at: http://www.ncbi.nlm.nih.gov/pubmed/9510251 [Accessed June 28, 2019]. [PubMed: 9510251]
8. Li X, Goel P, Chen C, Angajala V, Chen X, and Dickman DK (2018). Synapse-specific and compartmentalized expression of presynaptic homeostatic potentiation. Elife 7 Available at: http://www.ncbi.nlm.nih.gov/pubmed/29620520 [Accessed June 28, 2019].
9. Megías M, Emri Z, Freund TF, and Gulyás AI (2001). Total number and distribution of inhibitory and excitatory synapses on hippocampal CA1 pyramidal cells. Neuroscience.
10. Lnenicka GA, and Keshishian H (2000). Identified motor terminals inDrosophila larvae show distinct differences in morphology and physiology. J. Neurobiol 43, 186–197. Available at: http://doi.wiley.com/10.1002/%28SICI%291097-4695%28200005%2943%3A2%3C186%3A%3AAID-NEU8%3E3.0.CO%3B2-N [Accessed July 9, 2019]. [PubMed: 10770847]
11. Böhme MA, McCarthy AW, Grasskamp AT, Beuschel CB, Goel P, Jusyte M, Laber D, Huang S, Rey U, Petzoldt AG, et al. (2019). Rapid active zone remodeling consolidates presynaptic potentiation. Nat. Commun 10, 1085 Available at: http://www.nature.com/articles/s41467-019-08977-6 [Accessed June 25, 2019]. [PubMed: 30842428]
12. Gratz SJ, Goel P, Bruckner JJ, Hernandez RX, Khateeb K, Macleod GT, Dickman D, and O'Connor-Giles KM (2019). Endogenous Tagging Reveals Differential Regulation of Ca2+ Channels at Single Active Zones during Presynaptic Homeostatic Potentiation and Depression. J. Neurosci 39, 2416–2429. Available at: http://www.ncbi.nlm.nih.gov/pubmed/30692227 [Accessed May 15, 2019]. [PubMed: 30692227]
13. Li X, Goel P, Wondolowski J, Paluch J, and Dickman D (2018). A Glutamate Homeostat Controls the Presynaptic Inhibition of Neurotransmitter Release. Cell Rep. 23, 1716–1727. Available at: https://www.sciencedirect.com/science/article/pii/S2211124718305187?via%3Dihub [Accessed June 25, 2019]. [PubMed: 29742428]

14. Newman ZL, Hoagland A, Aghi K, Worden K, Levy SL, Son JH, Lee LP, and Isacoff EY (2017). Input-Specific Plasticity and Homeostasis at the Drosophila Larval Neuromuscular Junction. Neuron 93, 1388–1404.e10. Available at: https://www.sciencedirect.com/science/article/pii/S0896627317301368 [Accessed September 25, 2018]. [PubMed: 28285823]
15. Orr BO, Fetter RD, and Davis GW (2017). Retrograde semaphorin–plexin signalling drives homeostatic synaptic plasticity. Nature 550, 109–113. Available at: http://www.ncbi.nlm.nih.gov/pubmed/28953869 [Accessed April 26, 2018]. [PubMed: 28953869]
16. Müller M, Genç Ö, and Davis GW (2015). RIM-Binding Protein Links Synaptic Homeostasis to the Stabilization and Replenishment of High Release Probability Vesicles. Neuron 85, 1056–1069. Available at: http://www.ncbi.nlm.nih.gov/pubmed/25704950 [Accessed April 30, 2018]. [PubMed: 25704950]
17. Ortega JM, Genç Ö, and Davis GW (2018). Molecular mechanisms that stabilize short term synaptic plasticity during presynaptic homeostatic plasticity. Elife 7 Available at: http://www.ncbi.nlm.nih.gov/pubmed/30422113 [Accessed May 8, 2019].
18. Choi JC, Park D, and Griffith LC (2004). Electrophysiological and Morphological Characterization of Identified Motor Neurons in the Drosophila Third Instar Larva Central Nervous System. Available at: www.jn.org [Accessed September 25, 2018].
19. Pérez-Moreno JJ, and O'Kane CJ (2018). GAL4 Drivers Specific for Type Ib and Type Is Motor Neurons in Drosophila. G3: Genes|Genomes|Genetics 9, g3.200809.2018. Available at: http://www.ncbi.nlm.nih.gov/pubmed/30530644 [Accessed May 13, 2019].
20. Broihier HT, and Skeath JB (2002). Drosophila homeodomain protein dHb9 directs neuronal fate via crossrepressive and cell-nonautonomous mechanisms. Neuron 35, 39–50. Available at: http://www.ncbi.nlm.nih.gov/pubmed/12123607 [Accessed September 25, 2018]. [PubMed: 12123607]
21. Takizawa E, Komatsu A, and Tsujimura H (2007). Identification of Common Excitatory Motoneurons in Drosophila melanogaster Larvae. Zoolog. Sci 24, 504–513. Available at: http://www.bioone.org/doi/abs/10.2108/zsj.24.504 [Accessed May 4, 2018]. [PubMed: 17867850]
22. Berndt A, Schoenenberger P, Mattis J, Tye KM, Deisseroth K, Hegemann P, and Oertner TG (2011). High-efficiency channelrhodopsins for fast neuronal stimulation at low light levels. Proc. Natl. Acad. Sci. U. S. A 108, 7595–600. Available at: http://www.ncbi.nlm.nih.gov/pubmed/21504945 [Accessed June 3, 2019]. [PubMed: 21504945]
23. Lin JY, Knutsen PM, Muller A, Kleinfeld D, and Tsien RY (2013). ReaChR: a red-shifted variant of channelrhodopsin enables deep transcranial optogenetic excitation. Nat. Neurosci 16, 1499–1508. Available at: http://www.nature.com/articles/nn.3502 [Accessed June 3, 2019]. [PubMed: 23995068]
24. Kurdyak P, Atwood HL, Stewart BA, and Wu C-F (1994). Differential Physiology and Morphology of Motor Axons to Ventral Longitudinal Muscles in Larval DrosophiZa Available at: https://onlinelibrary.wiley.com/doi/pdf/10.1002/cne.903500310 [Accessed May 20, 2019].
25. Millar AG, Bradacs H, Charlton MP, and Atwood HL (2002). Inverse relationship between release probability and readily releasable vesicles in depressing and facilitating synapses. J. Neurosci 22, 9661–7. Available at: http://www.ncbi.nlm.nih.gov/pubmed/12427821 [Accessed May 21, 2019]. [PubMed: 12427821]
26. Lu Z, Chouhan AK, Borycz JA, Lu Z, Rossano AJ, Brain KL, Zhou Y, Meinertzhagen IA, and Macleod GT (2016). High-Probability Neurotransmitter Release Sites Represent an Energy-Efficient Design. Curr. Biol 26, 2562–2571. Available at: https://www.sciencedirect.com/science/article/pii/S0960982216307837?via%3Dihub [Accessed May 13, 2019]. [PubMed: 27593375]
27. Frank CA, Kennedy MJ, Goold CP, Marek KW, and Davis GW (2006). Mechanisms underlying the rapid induction and sustained expression of synaptic homeostasis. Neuron 52, 663–77. Available at: http://www.pubmedcentral.nih.gov/articlerender.fcgi?artid=2673733&tool=pmcentrez&rendertype=abstract [Accessed January 21, 2014]. [PubMed: 17114050]
28. Younger M a, Müller M, Tong A, Pym EC, and Davis GW (2013). A presynaptic ENaC channel drives homeostatic plasticity. Neuron 79, 1183–96. Available at: http://www.ncbi.nlm.nih.gov/pubmed/23973209. [PubMed: 23973209]
29. Genç Ö, Dickman DK, Ma W, Tong A, Fetter RD, and Davis GW (2017). MCTP is an ER-resident calcium sensor that stabilizes synaptic transmission and homeostatic plasticity. Elife 6, e22904

Available at: https://elifesciences.org/articles/22904 [Accessed January 23, 2018]. [PubMed: 28485711]

30. Marrus SB, Portman SL, Allen MJ, Moffat KG, and DiAntonio A (2004). Differential localization of glutamate receptor subunits at the Drosophila neuromuscular junction. J. Neurosci 24, 1406–15. Available at: http://www.ncbi.nlm.nih.gov/pubmed/14960613 [Accessed September 7, 2019]. [PubMed: 14960613]
31. Petersen SA, Fetter RD, Noordermeer JN, Goodman CS, and DiAntonio A (1997). Genetic analysis of glutamate receptors in drosophila reveals a retrograde signal regulating presynaptic transmitter release. Neuron 19, 1237–1248. [PubMed: 9427247]
32. Marie B, Pym E, Bergquist S, and Davis GW (2010). Synaptic homeostasis is consolidated by the cell fate gene gooseberry, a Drosophila pax3/7 homolog. J. Neurosci 30, 8071–82. Available at: http://www.ncbi.nlm.nih.gov/pubmed/20554858 [Accessed July 12, 2019]. [PubMed: 20554858]
33. Harris N, Fetter RD, Brasier DJ, Tong A, and Davis GW (2018). Molecular Interface of Neuronal Innate Immunity, Synaptic Vesicle Stabilization, and Presynaptic Homeostatic Plasticity. Neuron 100, 1163–1179.e4. Available at: http://www.ncbi.nlm.nih.gov/pubmed/30344041 [Accessed April 7, 2019]. [PubMed: 30344041]
34. Orr BO, Gorczyca D, Younger MA, Jan LY, Jan YN, and Davis GW (2017). Composition and Control of a Deg/ENaC Channel during Presynaptic Homeostatic Plasticity. Cell Rep.
35. Smith PD, Liesegang GW, Berger RL, Czerlinski G, and Podolsky RJ (1984). A stopped-flow investigation of calcium ion binding by ethylene glycol bis(beta-aminoethyl ether)-N,N'-tetraacetic acid. Anal. Biochem 143, 188–95. Available at: http://www.ncbi.nlm.nih.gov/pubmed/6442108 [Accessed September 27, 2016]. [PubMed: 6442108]
36. Schneggenburger R, and Neher E (2005). Presynaptic calcium and control of vesicle fusion. Curr. Opin. Neurobiol 15, 266–274. [PubMed: 15919191]
37. Ford KJ, and Davis GW (2014). Archaerhodopsin Voltage Imaging: Synaptic Calcium and BK Channels Stabilize Action Potential Repolarization at the Drosophila Neuromuscular Junction. J. Neurosci 34, 14517–14525. Available at: http://www.ncbi.nlm.nih.gov/pubmed/25355206 [Accessed January 31, 2017]. [PubMed: 25355206]
38. Lee T, and Luo L (1999). Mosaic analysis with a repressible neurotechnique cell marker for studies of gene function in neuronal morphogenesis. Neuron 22, 451–461. [PubMed: 10197526]
39. Mahr A, and Aberle H (2006). The expression pattern of the Drosophila vesicular glutamate transporter: A marker protein for motoneurons and glutamatergic centers in the brain. Gene Expr. Patterns 6, 299–309. [PubMed: 16378756]

Highlights

- Presynaptic homeostasis is uniformly induced at synapses contacting a single target
- Presynaptic homeostasis is differentially expressed at synapses on a single target
- Expression mechanisms change after transition from short to long-term plasticity
- Long-term homeostatic plasticity includes altered calcium-coupled vesicle release

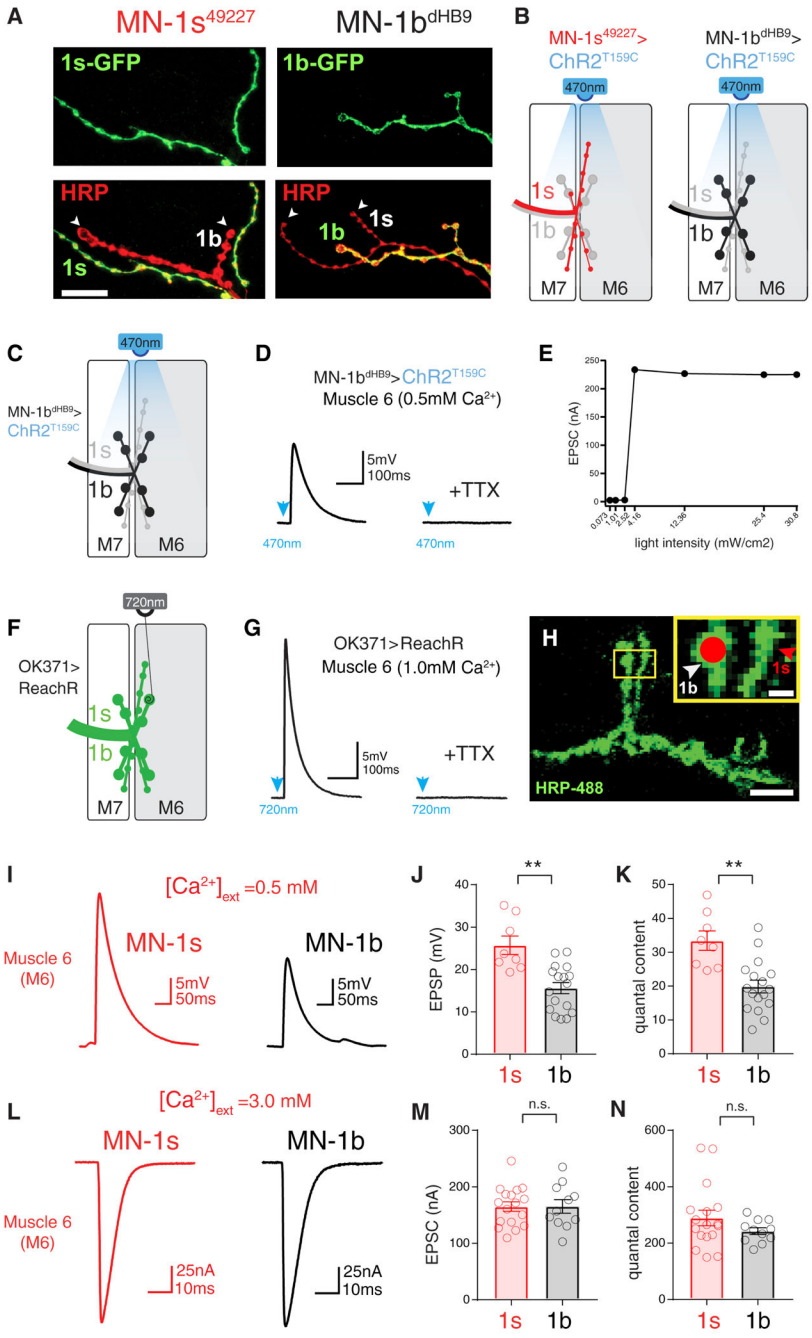

Figure 1. Selective stimulation of single motoneurons using ChR2.

(A) Example images showing the expression of *UAS-CD8-GFP* by MN-1s (left) and MN-1b (right) *GAL4* drivers. HRP staining (bottom panel, nerve terminal in red, highlighted with white arrow heads) uncovers the non-labeled MN-1b and MN-1s terminals for GFP. Scale bar: 50 μm **(B)** Muscle diagram showing the expression and illumination pattern of ChR2 for each MN type (red for MN-1s, black for MN-1b) at M6-M7. **(C)** NMJ diagram showing the expression of *UAS-ChR2^{T159C}* driven by *MN-1b^{dHB9}-Gal4* (black lines and circles). **(D)** Example traces of EPSPs recorded from M6 in the absence (left) and presence (right) of

tetrodotoxin (TTX) at 0.5 mM [Ca^{2+}]ext. **(E)** EPSC amplitudes (y-axis) plotted against corresponding light intensity values (x-axis) measured in the focal plane of the specimen. **(F)** NMJ diagram showing the expression of *UAS-ReachR* driven by *OK371-Gal4* (green lines and circles). **(G)** Example traces of EPSPs recorded from M6 in the absence (left) and presence (right) of tetrodotoxin (TTX - 1μM) at 1.0 mM [Ca^{2+}]ext. **(H)** 2-Photon image of an NMJ synapse stained live with conjugated HRP-488. Inset shows the bouton targeted by spiral scanning stimulation (white arrow head). Scale bar: 10 μm, inset 2 μm **(I)** Example traces of EPSPs recorded at M6 for MN-1s (left, red) and MN-1b (right, black) **(J-K)** Quantification of EPSP amplitudes and quantal content for MN-1s (n=8) and MN-1b (n=17). **(L)** Example traces of EPSCs recorded at M6 for MN-1s (left, red) and MN-1b (right, black) **(M-N)** Quantification of EPSC amplitudes and quantal content for MN-1s (n=17) and MN-1b (n=11). ** $p<0.01$, n.s. not significant, $p>0.05$; Data represent mean ±SEM. Student's t-test, two tailed. See also Figure S1 and S2.

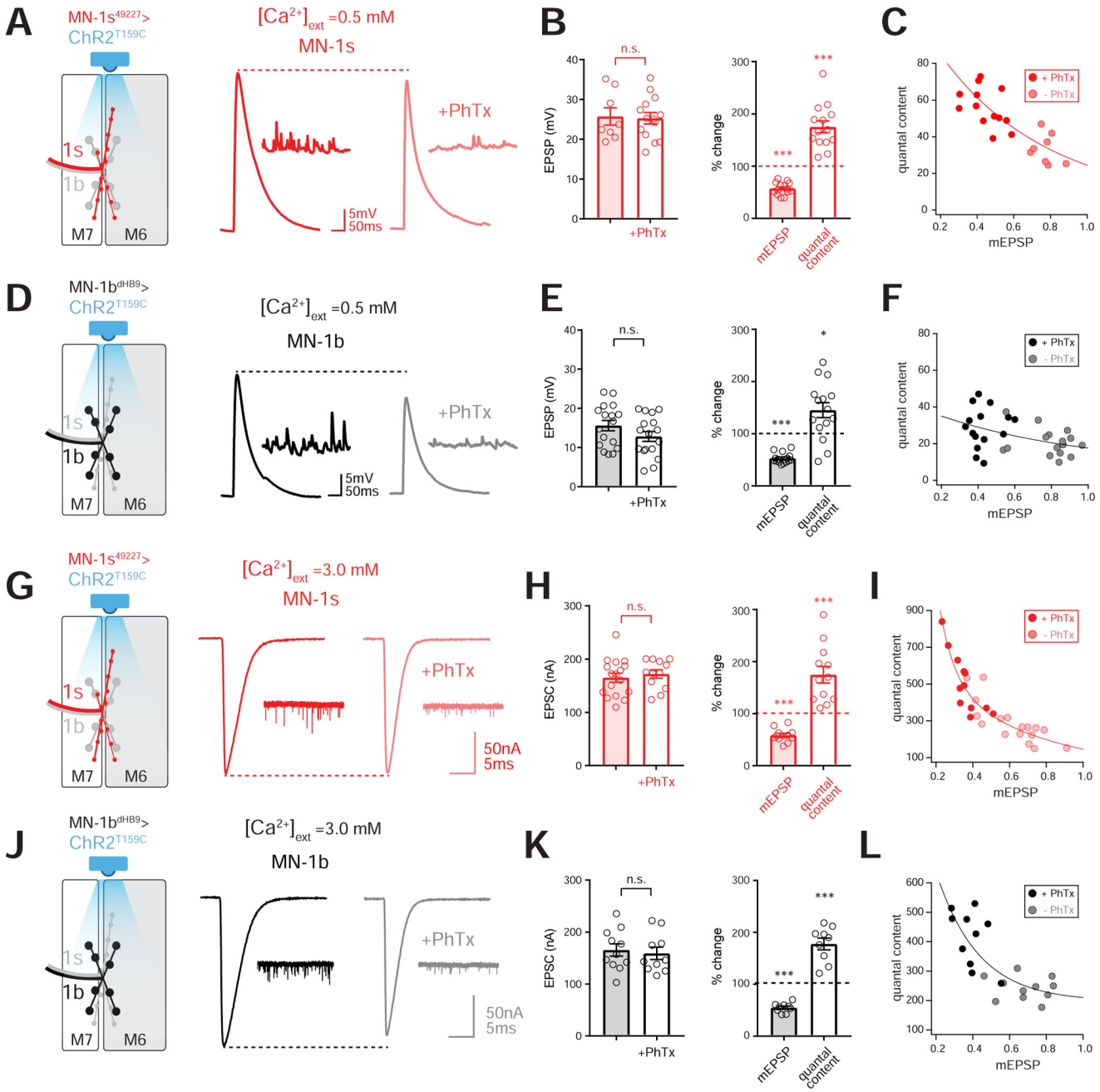

Figure 2. Uniform induction and differential expression of PHP and phasic and tonic synapses.

(A) NMJ diagram showing the expression of *UAS-ChR2*^{T159C} driven by *MN-1s-49227-Gal4* (red lines and circles) and example traces of EPSPs and mEPSPs recorded from M6 in the absence (red) and presence (pink) of philanthotoxin (PhTx) at 0.5 mM [Ca^{2+}]ext. **(B)** Quantification of EPSP amplitudes (baseline, pink bar; PhTx, open bar) and percent change in mEPSP amplitude (pink bar) and quantal content (open bar) in PhTx (n=14) compared to baseline (n=8). **(C)** Correlation plot of mEPSP amplitudes versus quantal content, fitted with an exponential function (red line). **(D-F)** Same display as **(A-C),** showing results from *MN-1b*^{dHB9}*-Gal4* driving *UAS-ChR2*^{T159C} (plots in black and gray tones). (PhTx, n=15;

baseline, n=17) **(G)** NMJ diagram showing the expression of *UAS-ChR2^{T159C}* driven by *MN-1s-49227-Gal4* (red lines and circles) and example traces of EPSCs and mEPSCs recorded from M6 in the absence (red) and presence (pink) of philanthotoxin (PhTx) at 3.0 mM [Ca^{2+}]ext. **(H)** Quantification of EPSC amplitudes (baseline, pink bar; PhTx, open bar) and percent change in mEPSP amplitude (pink bar) and quantal content (open bar) in PhTx (n=12) compared to baseline (n=17). **(I)** Correlation plot of mEPSP amplitudes versus quantal content, fitted with an exponential function (red line). **(J-L)** Same display as **(G-I),** showing results from *MN-1b^{dHB9}-Gal4* driving *UAS-ChR2^{T159C}* (plots in black and gray tones). (PhTx, n=10; baseline, n=11) n.s. not significant, p>0.05; Data represent mean ± SEM. Student's t-test, two tailed. See also Figure S3, S4 and S5.

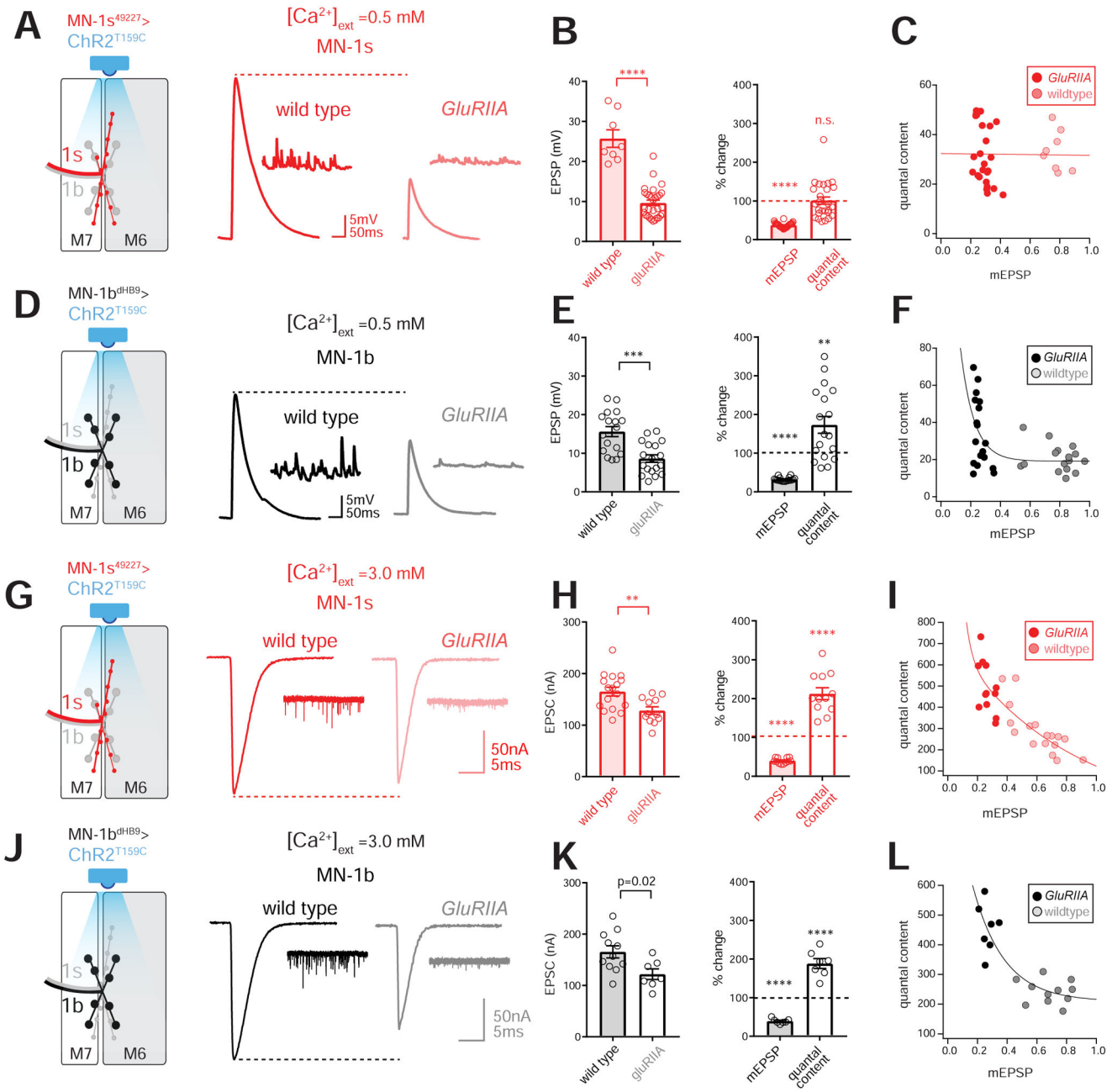

Figure 3. A switch in the synapse-specific expression of PHP

(A) NMJ diagram showing the expression of *UAS-ChR2^{T159C}* driven by *MN-1s-49227-Gal4* (red lines and circles) and example traces of EPSPs and mEPSPs recorded from M6 from wild type (red) and *GluRIIA* (pink) at 0.5 mM [Ca^{2+}]ext. **(B)** Quantification of EPSP amplitudes (wild type, pink bar; *GluRIIA*, open bar) and percent change in mEPSP amplitude (pink bar) and quantal content (open bar) for *GluRIIA* (n=26) compared to wild type (n=8). **(C)** Correlation plot of mEPSP amplitudes against quantal content, fitted with an exponential function (red line). **(D-F)** Same display as **(A-C),** showing results from *MN-1b^{dHB9}-Gal4* driver (plots in black and gray tones) (*GluRIIA*, n=18; wild type, n=17).

(G) NMJ diagram showing the expression of *UAS-ChR2^{T159C}* driven by *MN-1s-49227-Gal4* (red lines and circles) and example traces of EPSCs and mEPSCs recorded from M6 from wild type (red) and *GluRIIA* (pink) at 3.0 mM [Ca^{2+}]ext. **(H)** Quantification of EPSC amplitudes (wild type, pink bar; *GluRIIA*, open bar) and percent change in mEPSP amplitude (pink bar) and quantal content (open bar) for *GluRIIA* (n=12) compared to wild type (n=17). **(I)** Correlation plot of mEPSP amplitudes versus quantal content, fitted with an exponential function (red line). **(J-L)** Same display as **(G-I),** showing results from *MN-1b^{dHB9}-Gal4* driving expression of *UAS-ChR2^{T159C}* (plots in black and gray tones) (*GluRIIA*, n=7; wild type, n=11). ***p<0.001, ** p<0.01; Data mean ± SEM. Student's t-test, two tailed.

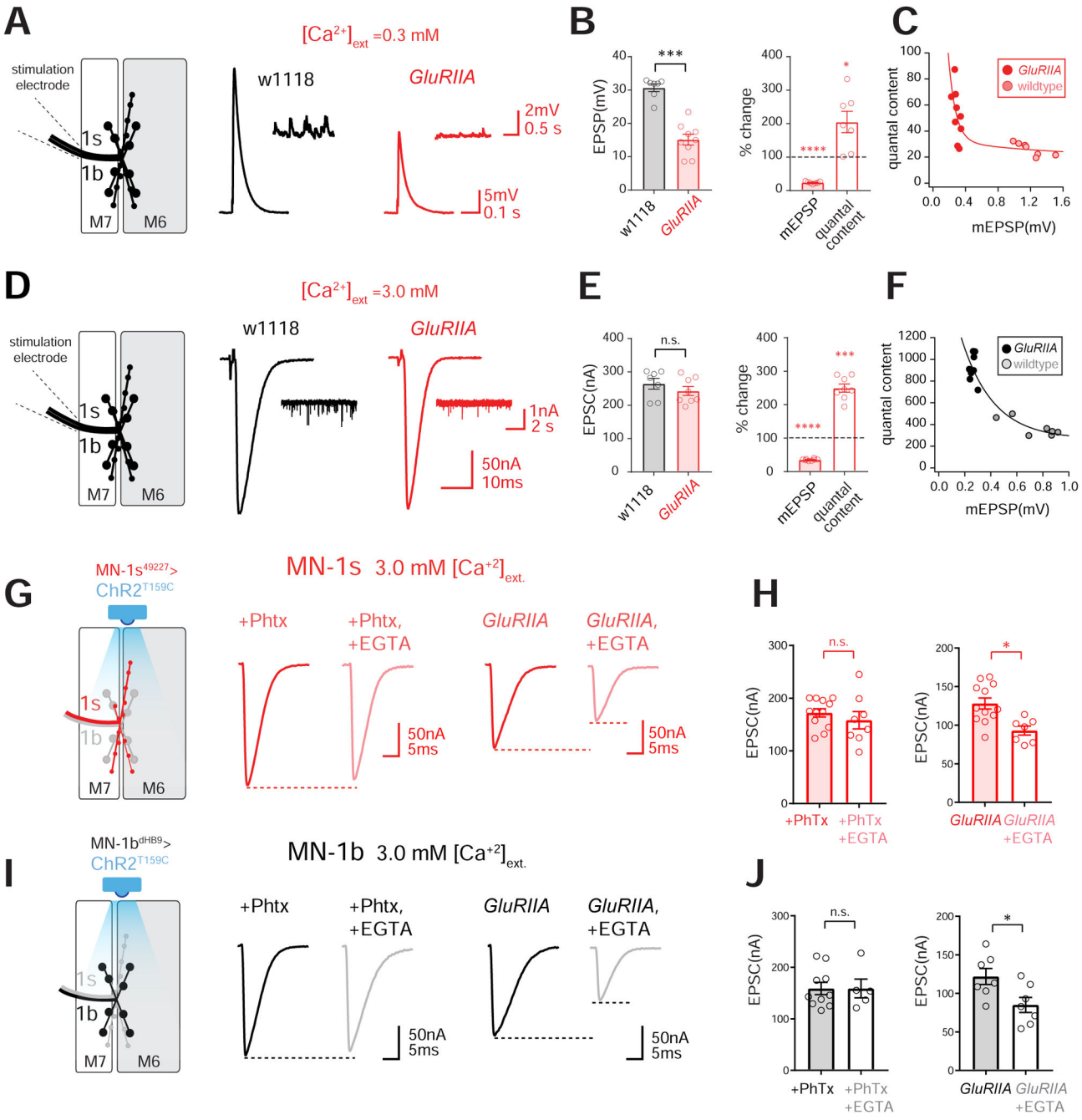

Figure 4. The long-term maintenance of PHP is an EGTA-sensitive process

(A) NMJ diagram showing the electrical stimulation of MN-1s and MN-1b nerve terminals (black lines and circles) and example traces of EPSPs and mEPSPs recorded from M6 from wild type (black) and *GluRIIA* (red) at 0.5 mM $[Ca^{2+}]$ext. **(B)** Quantification of EPSP amplitudes (wild type, gray bar, n=7; *GluRIIA*, red bar, n=9) and percent change in mEPSP amplitude (pink bar) and quantal content (open bar) for *GluRIIA* compared to wild type **(C)** Correlation plot of mEPSP amplitudes against quantal content, fitted with an exponential function (red line) **(D)** NMJ diagram showing the electrical stimulation of MN-1s and

MN-1b nerve terminals (black lines and circles) and example traces of EPSCs and mEPSCs recorded from M6 from wild type (black) and *GluRIIA* (red) at 3.0 mM $[Ca^{2+}]$ext. **(E)** Quantification of EPSC amplitudes (wild type, gray bar, n=7; *GluRIIA*, red bar, n=8) and percent change in mEPSP amplitude (pink bar) and quantal content (open bar) for *GluRIIA* compared to wild type **(F)** Correlation plot of mEPSP amplitudes against quantal content, fitted with an exponential function (red line) **(G)** NMJ diagram showing the expression of *UAS- ChR2*^{T159C} driven by *MN-1s-49227-Gal4* (red lines and circles) and example traces of EPSCs recorded from M6 with PhTx alone (red) and with PhTx and EGTA-AM together (pink) at 3.0 mM $[Ca^{2+}]$ext. **(H)** Quantification of EPSC amplitudes (On the left: PhTx, pink bar, n=11; PHTX+EGTA, open bar, n=8. On the right: *GluRIIA*, pink bar, n=12; *GluRIIA* +EGTA, n=7, open bar) **(I-J)** Same content as **(G-H)** showing results from MN-1b^{dHB9} driver (plots in black and gray tones, PhTx, n=11; PhTx+EGTA, n=5, *GluRIIA*, n=7; *GluRIIA*+EGTA, n=7, open bar). ***p<0.001, * p<0.05, n.s. not significant,; Data represent mean ±SEM. Student's t-test, two tailed

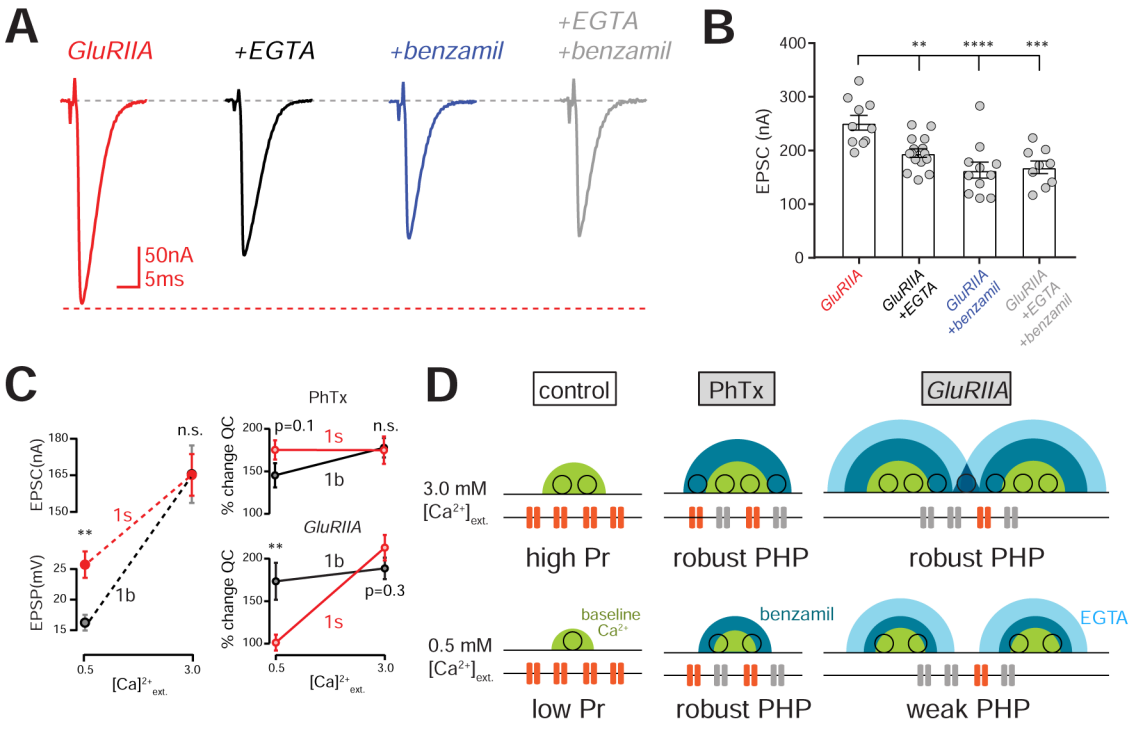

Figure 5. Differential synapse-specific expression of PHP.

(A) Example EPSC traces from *GluRIIA* (red), *GluRIIA*+EGTA (black), *GluRIIA*+benzamil (blue), *GluRIIA*+EGTA+benzamil (gray). **(B)** Quantification of EPSC amplitudes shown in (A) (*GluRIIA*, n=10; *GluRIIA*+EGTA, n=15; *GluRIIA*+benzamil, n=11; *GluRIIA*+EGTA +benzamil, n=9). **(C)** On the left panel, average EPSP and EPSC amplitudes (y-axis) from MN-1b (black circles) and MN-1s (red circles) plotted at 0.5 and 3.0 mM Ca^{2+} (x-axis). On the right panel, average percent change in quantal content (y-axis) from MN-1b (black circles) and MN-1s (red circles) plotted at 0.5 and 3.0 mM Ca^{2+} (x-axis) for PhTx (top) and for *GluRIIA* (bottom). **(D)** Model for acute and chronic expression of PHP at two different calcium concentrations as indicated. The top row diagrams a synapse at elevated extracellular calcium. Under control conditions, tightly coupled vesicles are released in response to action potential induced calcium entry (green domain). Application of PhTx poisons postsynaptic receptors (red-to-gray) and induces the ENaC channel-dependent, benzamil-sensitive increase in presynaptic calcium influx (blue), driving increased release of vesicles. In the *GluRIIA* mutant, an additional EGTA-sensitive component is achieved that accesses weakly coupled vesicles, elevating release. The bottom row proposes why PHP may fail at reduced external calcium in the *GluRIIA* mutant. Decreased calcium influx prevents access to weakly coupled vesicles rendering PHP more variable and causing PHP to fail at phasic synapses. Statistical analyses are One-Way ANOVA with Dunnett's multiple comparisons test with a single pooled variance

KEY RESOURCES TABLE

REAGENT or RESOURCE	SOURCE	IDENTIFIER
Antibodies		
Cy3-AffiniPure Goat Anti-Horseradish Peroxidase antibody	Jackson ImmunoResearch Labs	RRID: AB_2338959
Mouse Anti-Green Fluorescent Protein (GFP) Monoclonal Antibody, Unconjugated, Clone 3E6	Invitrogen (Thermo Fisher)	RRID: AB_221568
Alexa Fluor 488-AffiniPure Goat Anti-Horseradish Peroxidase	Jackson ImmunoResearch Labs	RRID: AB_2338965
Chemicals, Peptides, and Recombinant Proteins		
Philanthotoxin 433 tris(trifluoroacetate) salt	Santa Cruz Biotechnology	Cat# 255421, CAS 276684-27-6
Benzamil hydrochoride hydrate	Sigma Aldrich	Cat# B2417, CAS 161804-20-2
EGTA, Tetra(acetoxymethyl Ester)	Invitrogen	Cat# E1219
Tetrodotoxin citrate (TTX)	Tocris	Cat# 1078, CAS 18660-81-6
All-trans-retinal	Sigma Aldrich	Cat# R2500, CAS 116-31-4
Experimental Models: Organisms/Strains		
wild type (w1118)	Bloomington Drosophila Stock Center	Stock #3605
w; GluRIIA-SP16	[31]	PMID:9427247
w; Ok371-Gal4	[39]	PMID:16378756
w; GMR94G06-Gal4	Bloomington Drosophila Stock Center	Stock #40701
w; GMR27E09-Gal4	Bloomington Drosophila Stock Center	Stock #49227
w; dHB9-Gal4	[20]	PMID: 12123607
w; shakB-Gal4	[21]	PMID: 17867850
w; UAS-ChR2.T159C	Bloomington Drosophila Stock Center	Stock #58373
w; UAS-ReaChR	Bloomington Drosophila Stock Center	Stock #53741
w; UAS-mCD8:GFP	[38]	PMID: 10197526
Software and Algorithms		
Igor Pro 8.03	Wavemetrics	RRID:SCR_000325
Graphpad PRISM 7.04	Graphpad	RRID:SCR_002798
Adobe Illustrator CC 2018	Adobe	RRID:SCR_010279
MiniAnalysis 6.0.7	SynaptoSoft	RRID:SCR_002184
SlideBook 6	Intelligent Imaging	RRID:SCR_014300